Recursive Ultrasound Imaging

Nikolov, Svetoslav; Gammelmark, Kim; Jensen, Jørgen Arendt

Recursive ultrasound imaging

Svetoslav Nikolov, Kim Gammelmark, and Jørgen Arendt Jensen

Center for Fast Ultrasound Imaging, Department of Information Technology, Build. 344,
Technical University of Denmark, DK-2800 Lyngby, Denmark

Abstract

This paper presents a new imaging method, applicable for both 2D and 3D imaging. It is based on Synthetic Transmit Aperture Focusing, but unlike previous approaches a new frame is created after every pulse emission. The elements from a linear transducer array emit pulses one after another. The same transducer element is used after N_{xmt} emissions. For each emission the signals from the individual elements are beam-formed in parallel for all directions in the image. A new frame is created by adding the new RF lines to the RF lines from the previous frame. The RF data recorded at the previous emission with the same element are subtracted. This yields a new image after each pulse emission and can give a frame rate of e.g. 5000 images/sec.

The paper gives a derivation of the recursive imaging technique and compares simulations for fast B-mode imaging with measurements .

A low value of N_{xmt} is necessary to decrease the motion artifacts and to make flow estimation possible. The simulations show that for $N_{xmt} = 13$ the level of grating lobes is less than -50 dB from the peak, which is sufficient for B-mode imaging and flow estimation.

The measurements made with an off-line experimental system having 64 transmitting channels and 1 receiving channel, confirmed the simulation results. A linear array with a pitch of 208.5 μm, central frequency $f_{0tr} = 7.5$ MHz and bandwidth $BW = 70\%$ was used. The signals from 64 elements were recorded, beam-formed and displayed as a sequence of B-mode frames, using the recursive algorithm. An excitation with a central frequency $f_0 = 5$ MHz ($\lambda = 297$ μm in water) was used to obtain the point spread function of the system. The -6 dB width of the PSF is 1.056 mm at axial distance of 39 mm. For a sparse synthetic transmit array with $N_{xmt} = 22$ the expected grating lobes from the simulations are -53 dB down from the peak value at, positioned at $\pm28°$. The measured level was -51 dB at $\pm27°$ from the peak.

Images obtained with the experimental system are compared to the simulation results for different sparse arrays. The application of the method for 3D real-time imaging and blood-velocity estimations is discussed.

1 Introduction

Advances in DSP technology [1] make the real-time 3-D volumetric scanning a feasible imaging modality in medical ultrasound. Extending the traditional 2-D cross-sectional scanning to 3-D does not yield real-time imaging and new imaging methods have to be developed. The synthetic aperture techniques are attractive alternatives. They make it possible to increase the frame rate of B-mode ultrasound imaging, and obtain a dynamically focused image in both transmit and receive. The synthetic beam-formation approaches can be divided into three classes [1]:

- synthetic receive aperture [2]

- synthetic receive and transmit apertures [3], [4]

- synthetic transmit aperture [5],[6]

In synthetic aperture imaging the time needed to acquire a single high-resolution image (HRI) T_{HRI} is proportional to the number of emissions N_{xmt}, the time necessary to record the reflected ultrasound wave from a single emission T_{rec}, and the number of scan-lines N_l. It is inversely proportional to the number of the parallel receive beam-formers N_{prb}:

$$T_{HRI} = T_{rec} \cdot N_{xmt} \cdot N_l / N_{prb} \qquad (1)$$

Synthetic receive processing involves transmitting with a full aperture and receiving with two or more sub-arrays. Several emissions are needed for every scan-line, thus, increasing T_{HRI}[1].

In contrast to synthetic receive aperture processing, synthetic transmit aperture imaging involves transmission from two or more sub-apertures and receiving with a full array. In receive the RF signals from the transducer elements can be beam-formed simultaneously for all directions in the image, i.e. $N_{prb} = N_l$ [5], [6]. For every emission a low-resolution image (LRI) is created. After acquiring N_{xmt} low-resolution images, the RF lines of these images are added together to form a single high-resolution image. The acquisition time for a LRI with a typical depth of 15 cm, assuming a speed of sound $c = 1540$ m/s, is $T_{rec} = 200$ μs. If $N_{xmt} = 64$, then $T_{HRI} = 12.8$ ms, and the frame rate is 78 frames/sec. This

paper suggests further development of the transmit synthetic processing. Instead of discarding the already created high-resolution image and starting the imaging procedure all over again, the next high-resolution image is recursively built from the previous one by adding the beam-formed RF-lines from the next low-resolution image to the existing high-resolution RF-lines. The RF-lines from the low-resolution image obtained at the previous emission of the current transmit sub-aperture are subtracted from the result.

The suggested recursive calculation procedure makes it possible to create a new high-resolution image at every pulse emission, i.e. $N_{xmt} = 1$ and, thus, increase the frame rate up to 5000 frames/sec.

2   Recursive ultrasound imaging

Phased linear arrays are used to create sector B-mode images. The image consists of N_l scan-lines with common origin. Each scan-line l is defined by the angle with the normal vector to the transducer surface θ_l.

A pulse emitted by only one transducer element propagates as a spherical wave, when the element is small, and the received echo signal carries information from the whole region of interest. By applying different delays in receive, *any* of the scan-lines $l \in [1 \ldots N_l]$ can be formed. The data from one emission is used to beam-form *all* of the scan-lines creating one image as shown in Fig. 1. The created image has a low resolution, since only one element is used for emission. A high-resolution image is created by summing the RF lines from N_{xmt} low resolution images, each of them created after emitting with a different transducer element. Let the number of the current emission be n, the number of the transducer elements be N_{xdc}, the recorded signal by the element j after emitting with element i be $r_{ij}^{(n)}$, and let the necessary delay and the weighting coefficient for beam-forming scan-line l be respectively d_{lij} and a_{lij}. The beam-forming of a scan-line for a low-resolution image can then be expressed as (see Fig. 1):

$$s_{li}^{(n)}(t) = \sum_{j=1}^{N_{xdc}} a_{lij} \cdot r_{ij}^{(n)}(t - d_{lij}), \tag{2}$$

where t is the time relative to the start of pulse emission. The number of skipped elements between two consecutive transmissions $n-1$ and n is:

$$N_{skip} = \text{floor}[(N_{xdc} - N_{xmt})/(N_{xmt} - 1)] \tag{3}$$

If $N_{xdc} = 64$ and $N_{xmt} = 4$ then $N_{skip} = 20$. The values for N_{xdc} should be a multiple of N_{xmt}, so that N_{skip} is an integer number.

The relation between the index i of the emitting element and the number n of the emission is given by:

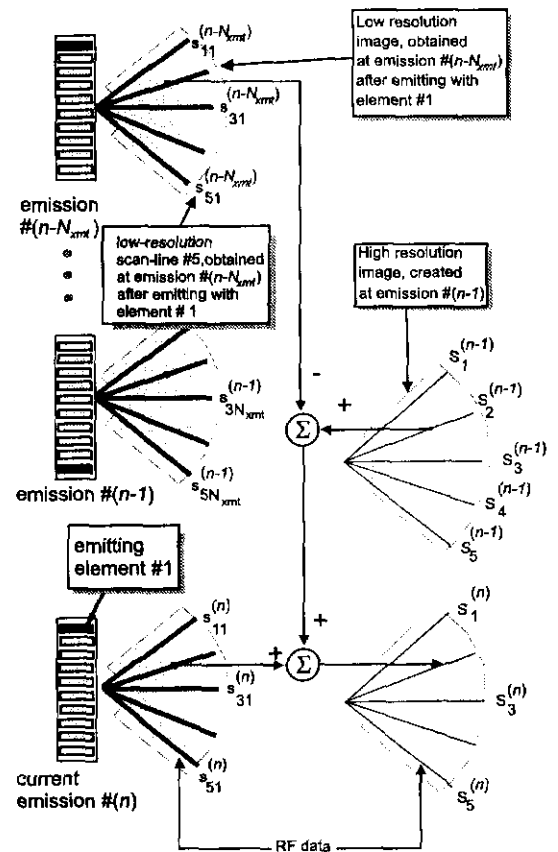$$i = [((n-1) \cdot (N_{skip} + 1)) \bmod N_{xdc}] + 1 \tag{4}$$

Figure 1: Recursive ultrasound imaging. In transmit only one element is excited. Multiple receive beams are formed simultaneously for each transmit pulse. Each element is excited again after N_{xmt} emissions ($N_{xmt} = N_{xdc} = 10$ in this example).

If $N_{skip} = 20$ then $i = 1, 22, 43, 64, 1, \cdots$. It can be seen that emissions n and $n \pm N_{xmt}$, are done by the same transducer element.

The forming of the final scan-lines for the high-resolution image can be expressed as:

$$S_l^{(n)}(t) = \sum_{k=n-N_{xmt}+1}^{n} s_{li}^{(k)}(t) \tag{5}$$

Equation (5) implies that a high-resolution image can be formed at any emission n, provided that N_{xmt} low-resolution images already exist. The images that will be formed at emissions n and $n-1$ can be expressed as:

$$S_l^{(n)}(t) = \sum_{k=n-N_{xmt}+1}^{n} s_{li}^{(k)}(t) \tag{6}$$

$$S_l^{(n-1)}(t) = \sum_{k=n-N_{xmt}}^{n-1} s_{li}^{(k)}(t) \tag{7}$$

Subtracting $S_l^{(n-1)}(t)$ from $S_l^{(n)}(t)$ gives:

$$S_l^{(n)}(t) = S_l^{(n-1)}(t) + s_{li}^{(n)}(t) - s_{li}^{(n-N_{xmt})}(t) \qquad (8)$$

In (8) the new high-resolution scan-line depends on the low-resolution scan-lines at emissions n and $n - N_{xmt}$, and on the high-resolution scan-line at emission $n - 1$. This dependence can be extended over a number of low- and high- resolution scan-lines obtained at previous emissions, and Equation (8) can be generalized as:

$$S_l^{(n)}(t) = \sum_{k=1}^{B} c_k \cdot S_l^{(n-k)}(t) + \sum_{q=0}^{Q} b_q \cdot s_{li}^{(n-q)}(t), \qquad (9)$$

where B and Q are respectively the number of high- and low-resolution scan-lines on which $S_l^{(n)}$ depends, and c_k and b_q are weighting coefficients. The recursive imaging procedure uses information from previous emissions and therefore suffers from motion artifacts. They can be reduced by decreasing Q or/and B and in this way trading resolution for motion artifacts. If $B = 1$ and $Q = 0$, the imaging procedure becomes *add-only recursive imaging*.

3 Add-only recursive imaging

Let B and Q in (9) be respectively 1 and 0. The calculation procedure becomes:

$$S_l^{(n)}(t) = c_1 \cdot S_l^{(n-1)}(t) + b_0 \cdot s_{li}^{(n)}(t) \qquad (10)$$

The difference between equations (8) and (10) is that instead of being subtracted, the information obtained after the emission with element i decays exponentially with time. In this way the information from the past is less prone to introduce motion artifacts in the image. The other benefit is that less memory is needed, since only two frames are stored. The high-resolution image is created by only adding weighted low-resolution images. This process starts at emission $n = 1$. Let all of the transducer elements participate in creating the synthetic transmit aperture ($N_{xmt} = N_{xdc}$). At emission n the high-resolution image is a weighted sum of all the low-resolution images obtained at the emissions with the single elements. Consider only the low-resolution images obtained after emissions with element i. The first emission with element i is $n = i$. The second emission with the same element is $n = i + N_{xmt}$. Element i is used after every N_{xmt} emissions. The sum C_{li} of the low-resolution scan-lines $s_{li}^{(n)}$ obtained at these emissions will be called *partially beam-formed scan-line C_{li}*. The high-resolution scan-lines are a sum of the partially beam-formed scan lines :

$$S_l(t) = \sum_{i=1}^{N_{xmt}} C_{li}(t) \qquad (11)$$

System parameter	Notation	Value	Unit
Speed of sound	c	1540	m/s
Central frequency	f_0	3	MHz
Sampling frequency	f_s	105	MHz
Oscillation periods	N_{osc}	3	
Pitch	$pitch$	0.257	mm
Number of elements	N_{xdc}	64	
Relative two-sided -6 dB bandwidth	B	70	%

Table 1: Simulation parameters for a 3 MHz phased array system.

N_{xmt}	$N_{act} = 1$ Position	Level	$N_{act} = 11$ Position	Level
64	NA	NA	NA	NA
22	$\pm 40°$	-58 dB	$\pm 40°$	-58 dB
13	$\pm 21°$	-54 dB	$\pm 21°$	-53 dB
8	$\pm 13°$	-48 dB	$\pm 13°$	-47 dB

Table 2: The position and level of the first grating lobe as a function of the number of emissions N_{xmt}.

If $b_0 = 1$, then the partially beam-formed scan-line for element i, $C_{li}^{(n)}$ at emission n is:

$$C_{li}^{(n)}(t) = s_{li}^{(n)}(t) + c_1^{N_{xmt}} \cdot s_{li}^{(n-N_{xmt})}(t) + c_1^{2N_{xmt}} \cdot s_{li}^{(n-2N_{xmt})}(t) + \cdots \qquad (12)$$

This is a geometric series. If the tissue is motionless then:

$$s_{li}^{(n)}(t) = s_{li}^{(n-N_{xmt})}(t) = \cdots = s_{li}(t) \qquad (13)$$

$$C_{li}^{(n)}(t) = [1 + c_1^{N_{xmt}} + c_1^{2N_{xmt}} + \cdots]s_{li}(t) \qquad (14)$$

$$C_{li}^{(n)}(t) = s_{li}(t) \cdot \frac{1}{1 - c_1^{N_{xmt}}} \qquad (15)$$

If $c_1 = 0.9$ and $N_{xmt} = 64$ then $1/(1 - c^{N_{xmt}}) \approx 1$ and $C_{li}^{(n)}(t) \approx s_{li}^{(n)}(t)$. Substituting the result in (11) gives the following result for the high-resolution scan-line:

$$S_l^{(n)}(t) \approx \sum_{i=0}^{N_{xmt}-1} c_1^i \cdot s_{li}^{(n-i)}(t) \qquad (16)$$

Using (16) for imaging, instead of (8) gives images with lower resolution due to the weighting in the sum. In this case the resolution is traded for motion artifacts and less memory storage requirements, which is beneficial for flow estimation.

4 Simulation results

Simulations were done to evaluate the performance of the imaging system as a function of the number of emissions

System parameter	Notation	Value	Unit
Speed of sound	c	1485	m/s
Central frequency	f_0	5	MHz
Sampling frequency	f_s	40	MHz
Oscillation periods	N_{osc}	3	
Pitch	$pitch$	0.2085	mm
Number of elements	N_{xdc}	64	
Relative two-sided -6 dB bandwidth	BW	70	%

Table 3: Parameters of the EXTRA measurement system [8]. The same parameters were used in simulations to obtain the expected levels and positions of the grating lobes

N_{xmt}	Expected Position	Level	Measured Position	Level
64	NA	NA	NA	NA
13	$\pm 15°$	-53 dB	± 17	-51 dB
8	$\pm 8°$	-47 dB	± 10	-44.5 dB

Table 4: Measured versus expected grating lobe position and level for $N_{act} = 11$.

N_{xmt}. Equation (8) was used to create high-resolution images of the point spread function.

All the simulations were done with the program Field II [7]. The parameters are listed in Table 1.

The beam-formed signal was decimated 10 times and then envelope detected by a Hilbert transformation. The envelope of the signal was logarithmically compressed with a dynamic range of 60 dB. Since the B-mode image is a sector image, the point spread function was obtained by taking the maximum of the reflected signal from every direction. In the first simulation only one element ($N_{act} = 1$) was used for a single emission. The -6 dB width of the acquired point-spread-function was $1.01°$ and the -40 dB width was $5.03°$. The levels and positions of the grating lobes as a function of the number of emissions N_{xmt} are shown in Table 2. The simulations, however, did not account for the attenuation of the signal and the presence of noise. For real applications the energy sent into the body at one emission must be increased. One way is to use multiple elements whose delays are set to create a spherical wave [5]. To verify the method, simulations with 11 active elements forming a spherical wave at every transmission, were done. The width of the point-spread-function was identical to the one obtained with $N_{act} = 1$. The levels and positions of the grating lobes are given in Table 2. These results show that the radiation pattern of a single element can be successfully approximated by using several elements to increase the signal-to-noise ratio.

One of the problems, accompanying all synthetic aperture techniques are motion artifacts, and simulations with mov-
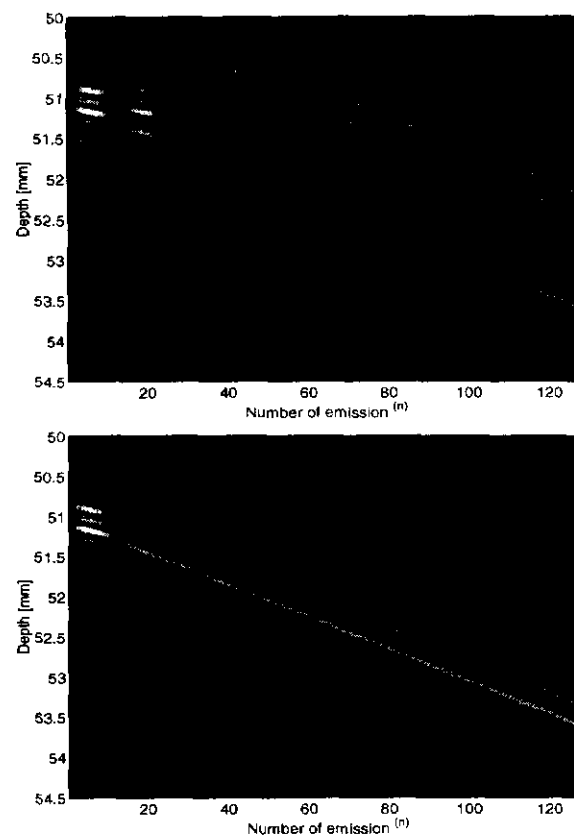

Figure 2: The development of a single high-resolution scanline as a function of the number of emissions n for normal recursive imaging (top), and for add-only recursive imaging (bottom).

ing scatterers were therefore done. The signal from a single point scatterer moving at a constant speed $v = 0.1$ m/s away from the transducer was simulated. The simulation parameters were the same as those in Table 1 except for the number of oscillation which in this case were $N_{osc} = 5$. The pulse repetition frequency was $f_{prf} = 5000$ Hz. Figure 2 shows one RF-line of the high-resolution image as a function of the number of emissions n. From Fig. 2, top it can be seen that the recursive imaging procedure suffers from motion artifacts as the other synthetic focusing algorithms. However, it can be seen from Fig. 2, bottom that these artifacts are reduced for the add-only recursive imaging and it can be used for velocity estimations.

5 Experimental results

The measurements were done with the off-line experimental system EXTRA [8] in a water tank and on a wire phantom with attenuation. The parameters of the system are listed in Table 3. The transducer was a linear array with a pitch
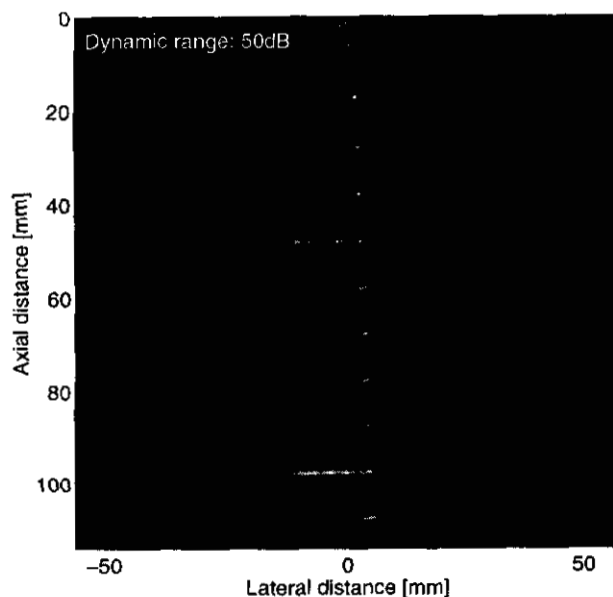
Figure 3: Synthetic image of a wire phantom.

$p = \lambda$. These parameters differ from the desired ($p = \lambda/2$), and new simulations were made in order to determine the expected point-spread-function, and to compare it to the measured one. The expected −6 dB width point-spread-function was 1.38° and the −40 dB width was −4.4°. The expected positions and levels of the grating lobes are given in Table 4. The results of the measurements are in good agreement with the simulation results. The result of scanning a wire phantom is given in Fig. 3. This image was obtained using 11 elements at every emission. The phantom has a frequency dependent attenuation of 0.25 dB · (cm · MHz)$^{-1}$. The focusing delays are calculated for every scan-line sample, and the two-way propagation time of the acoustic wave is taken into consideration. Therefore the image has the quality of a dynamically focused in transmit and receive image.

6 Conclusions

A new fast imaging method has been presented. The created images have the quality of dynamically focused image in transmit and receive. The time necessary to create one frame is equal to the time of acquisition of a single scan line in the conventional scanners. The signal-to-noise ratio can be increased by using multiple elements in transmit. The motion artifacts are decreased by add-only recursive imaging and the acquired information can be used for velocity estimations.

Some of the possible applications of the method are in the real-time three-dimensional imaging and blood velocity vector estimation.

The method can be further optimized by the use of coded excitations to increase the penetration depth and the signal-to-noise ratio.

7 Acknowledgement

References

[1] K. E. Thomenius. Evolution of ultrasound beamformers. In *Proc. IEEE Ultrason. Symp.*, pages 1615–1621, 1996.

[2] L. F. Nock and G. E. Trahey. Synthetic receive aperture imaging with phase correction for motion and for tissue inhomogenities - part 1: basic principles. *IEEE Trans. Ultrason., Ferroelec., Freq. Contr.*, 39:489–495, 1992.

[3] M. Kraman, P. Li, and M. O'Donnel. Synthetic aperture imaging for small scale systems. *IEEE Trans. Ultrason., Ferroelec., Freq. Contr.*, 42:429–442, 1995.

[4] J. T. Ylitalo and H. Ermert. Ultrasound synthetic aperture imaging: monostatic approach. *IEEE Trans. Ultrason., Ferroelec., Freq. Contr.*, 41:333–339, 1994.

[5] G. R. Lockwood, J. R. Talman, and S. S. Brunke. Real-time 3-D ultrasound imaging using sparse synthetic aperture beamforming. *IEEE Trans. Ultrason., Ferroelec., Freq. Contr.*, 45:980–987, 1998.

[6] G. R. Lockwood and F. S. Foster. Design of sparse array imaging systems. In *Proc. IEEE Ultrason. Symp.*, pages 1237–1243, 1995.

[7] J. A. Jensen. Field: A program for simulating ultrasound systems. *Med. Biol. Eng. Comp.*, 10th Nordic-Baltic Conference on Biomedical Imaging, Vol. 4, Supplement 1, Part 1:351–353, 1996b.

[8] S. K. Jespersen, J. E. Wilhjelm, and H. Sillesen. Multi-angle compound imaging. *Ultrason. Imaging*, 20:81–102, 1998.